THE JOURNAL OF BIOLOGICAL CHEMISTRY VOL. 282, NO. 9, pp. 6347–6355, March 2, 2007
© 2007 by The American Society for Biochemistry and Molecular Biology, Inc. Printed in the U.S.A.

pH Dependence of Copper Geometry, Reduction Potential, and Nitrite Affinity in Nitrite Reductase*

Received for publication, June 15, 2006, and in revised form, November 22, 2006 Published, JBC Papers in Press, December 5, 2006, DOI 10.1074/jbc.M605746200

Frida Jacobson[‡], Arthur Pistorius[§1], Daniel Farkas[¶], Willem De Grip[§2], Örjan Hansson[¶], Lennart Sjölin[‖], and Richard Neutze[‡3]

From the[‡]Department of Chemical and Biological Engineering, Chalmers University of Technology, Box 462, SE-40530 Göteborg, Sweden,[§]Department of Biochemistry, UMC-286, Nijmegen Centre for Molecular Life Sciences, Radboud University Nijmegen Medical Centre, P. O. Box 9101, 6500 HB Nijmegen, The Netherlands, [¶]Biochemistry and Biophysics, Department of Chemistry, Göteborg University, Box 462, SE-40530 Göteborg, Sweden, and [‖]Inorganic Chemistry, Department of Chemistry, Göteborg University, SE-41296 Göteborg, Sweden

Many properties of copper-containing nitrite reductase are pH-dependent, such as gene expression, enzyme activity, and substrate affinity. Here we use x-ray diffraction to investigate the structural basis for the pH dependence of activity and nitrite affinity by examining the type 2 copper site and its immediate surroundings in nitrite reductase from *Rhodobacter sphaeroides 2.4.3*. At active pH the geometry of the substrate-free oxidized type 2 copper site shows a near perfect tetrahedral geometry as defined by the positions of its ligands. At higher pH values the most favorable copper site geometry is altered toward a more distorted tetrahedral geometry whereby the solvent ligand adopts a position opposite to that of the His-131 ligand. This pH-dependent variation in type 2 copper site geometry is discussed in light of recent computational results. When co-crystallized with substrate, nitrite is seen to bind in a bidentate fashion with its two oxygen atoms ligating the type 2 copper, overlapping with the positions occupied by the solvent ligand in the high and low pH structures. Fourier transformation infrared spectroscopy is used to assign the pH dependence of the binding of nitrite to the active site, and EPR spectroscopy is used to characterize the pH dependence of the reduction potential of the type 2 copper site. Taken together, these spectroscopic and structural observations help to explain the pH dependence of nitrite reductase, highlighting the subtle relationship between copper site geometry, nitrite affinity, and enzyme activity.

The nitrogen cycle has received much attention in recent years due to the fact that several substrates and products of the pathway are known to be environmental pollutants (1). In dissimilatory denitrification (2), nitrate is used as an alternative electron acceptor during respiration when oxygen is scarce, being reduced stepwise and finally returned to the biosphere as inorganic nitrogen. One of the intermediate compounds is $NO_{(g)}$, which is toxic to the host at high levels. It is, therefore, of great importance for the bacteria to regulate the concentration of NO. This regulation is achieved by the controlled expression of two enzymes, nitrite reductase (NiR)[4] and NO reductase. NiR reduces nitrite to produce $NO_{(g)}$, and NO reductase reduces NO to N_2O, where NO is the first gaseous compound in the pathway. There are two main categories of NiRs; those that are heme-containing (cd1-NiRs) (3, 4) and those that are copper-containing (Cu-NiRs) (5–8). The overall enzymatic reaction performed by NiRs is $NO_2^- + 2H^+ + e^- \rightarrow NO_{(g)} + H_2O$.

Cu-NiRs are blue or green in color, showing visible absorption at 460 and 600 nm (1). The relative magnitude of these absorption peaks determines the enzyme color (*i.e.* blue or green). RsNiR is a copper-containing green NiR with two peaks of equal maximum absorption at 457 and 590 nm (9). As with all other Cu-NiRs, the protein is a homotrimer with two copper atoms per monomer, ~12 Å apart. The type 1 copper site has four ligands (His-126, His-177, Cys-167, and Met-182) and is located a few angstroms beneath a hydrophobic surface (8), which is the docking site for an electron donor protein (10, 11). The type 2 copper site is situated at the monomer-monomer interfaces and has ligands from both monomers (His A131, His A166, His B338), forming a propeller-shaped structure with the copper at its center. When the type 2 copper is oxidized, there is also a fourth ligand, a solvent molecule, but this ligand disorders upon reduction of the type 2 copper ion (12, 13).

Nitrite binds directly to the type 2 copper ion (14), with both oxygen atoms ligating the copper site in a bidentate fashion (6, 13). After an electron is passed to the type 1 copper site from the electron donor protein, the electron is transferred on to nitrite via the type 2 copper ion (15). Although schematics of the enzymatic reaction typically only mention the species NO_2^-, it has

* This work was supported by Swedish Natural Science Research Council and Stint. The costs of publication of this article were defrayed in part by the payment of page charges. This article must therefore be hereby marked "*advertisement*" in accordance with 18 U.S.C. Section 1734 solely to indicate this fact.

The atomic coordinates and structure factors (code 2DWS, 2DY2, and 2DWT) have been deposited in the Protein Data Bank, Research Collaboratory for Structural Bioinformatics, Rutgers University, New Brunswick, NJ (http://www.rcsb.org/).

[1] Supported by the Chemical Council of the Netherlands Organization for Scientific Research (NWO-CW).

[2] Supported by the Chemical Council of the Netherlands Organization for Scientific Research (NWO-CW) and by European Union Grant LSHG-CT-2004-504601 (to the E-Mep consortium).

[3] To whom correspondence should be addressed. E-mail: richard.neutze@chembio.chalmers.se; Tel.: 46-31-7733974; Fax: 46-31-7733910.

[4] The abbreviations used are: NiR, nitrite reductase; Cu-NiR, copper-containing nitrite reductase; RsNiR, nitrite reductase from *R. sphaeroides 2.4.3*; FTIR, Fourier transformation infrared spectroscopy; MES, 4-morpholineethanesulfonic acid; PEG, polyethylene glycol.

Downloaded from www.jbc.org at Radboud Universiteit Nijmegen, on July 12, 2012

TABLE 1
Crystallization conditions for the structures of RsNiR at pH 6.0 and 8.4 with and without nitrite

	pH 8.4[a]	pH 8.4 + NO_2^-	pH 6.0	pH 6.0 + NO_2^-
PEG	19% PEG 4000	16% PEG 4000	29% PEG 1500	29% PEG 1500
$MgCl_2$	0.24 M	0.15 M	0.32 M	0.32 M
$NaNO_2$		5 mM	-	10 mM in protein solution
Protein concentration	0.1 mM	0.1 mM	0.15 mM	0.1 mM
Buffer (type + concentration)	100 mM Tris (pH 8.4)	100 mM Tris (pH 8.4)	100 mM MES (pH 6.0)	100 mM MES (pH 6.0)
PDB code	1ZV2	2DWS	2DY2	2DWT

[a] From Jacobson *et al.* (12).

been argued that it is actually the protonated HNO_2 species that binds to the active site (16, 17). Recent studies have shown that before the $NO_{(g)}$ product leaves the type 2 copper site, it is bound to the copper ion as a side-on copper-nitrosyl intermediate (17, 18). Near the type 2 site there are also the catalytic residues Asp-129 and His-287, which have been found to be crucial to enzyme activity and nitrite binding (9, 16, 19–22). These residues are bridged by a solvent molecule referred to as the "bridging water," and Asp-129 forms an H-bond to one of the oxygen atoms when nitrite is bound or to the water ligand in the absence of nitrite (6). All details concerning the catalytic role of His-287 are not entirely clear, but this residue is believed to be involved in supplying the proton needed for the enzymatic reaction to occur (6) and has in *Rhodobacter sphaeroides* been seen to disorder at high pH, most likely due to loss of H-bond interactions (12).

Nitrite reductase is highly pH-dependent and has an activity maximum between pH 5 and 6 (23, 24). One property influencing the activity of NiR is the active-site affinity of the substrate, which in turn varies with pH (25). It has also been reported that *nirK*, the gene encoding Cu-NiRs (2), is regulated by both nitrite concentrations and pH in such a way that high nitrite concentrations increases the expression of *nirK*, whereas increased pH down-regulates the expression of this gene, as indicated by recent findings for *nirK* from *Nitrosomonas europaea* (26). This correlation between the pH dependence of the expression levels and activity emphasizes the fact that nitrite production is strictly controlled within the cell. In this work we use x-ray crystallography to identify those structural features of NiR that are pH-dependent, and we correlate these findings with data from EPR and FTIR spectroscopy to characterize the structural causes and implications of the pH-dependent activity of RsNiR. Our results highlight the elegant way in which nature has exploited subtle pH-dependent differences in the ligating properties of metal centers to regulate the activity of copper-dependent enzymes.

MATERIALS AND METHODS

Nitrite reductase was expressed in *Escherichia coli* and purified as described (12). Protein crystals were grown using the hanging drop vapor diffusion method at 293 K. Crystallization was performed with and without nitrite at both pH 6.0 and 8.4. The protein concentration ranged from 0.1 to 0.15 mM. Nitrite was added to the well solution in the case of pH 8.4, but when crystallized at pH 6.0 nitrite was only added to the protein solution before setting up the drops. For cryoprotection, solutions containing 10% PEG 400 were prepared from the specific crystallization conditions. The crystallization conditions can be found in Table 1.

Data were collected at the MAXLAB II synchrotron facility in Lund, Sweden, at beamline I7-11/I9-11. Indexing and integration of the data were performed with Mosfilm (27), and scaling and merging were performed with Scala (28) in the CCP4 program suite (29). The structures were solved with molecular replacement using AMoRe (30) or MOLREP (31) using another RsNiR structure as a model (Protein Data Bank code 1ZV2). For all datasets refinement was carried out in CCP4 (Refmac 5 (32)) and CNS, and subsequent model rebuilding was performed in O (33). After molecular replacement, a rigid body refinement was performed with Refmac 5 followed by a round of restrained refinement. The copper atoms were then added to the model, and two rounds of simulated annealing were carried out in CNS. Solvent molecules were added after simulated annealing with ARP/Warp (34) during refinement in Refmac 5, and the rest of the refinement and model building was done in Refmac 5 and in O, respectively.

In the dataset obtained from RsNiR co-crystallized with substrate at pH 6.0, nitrite was modeled (at the end of refinement) into two $F_o - F_c$ difference electron density peaks, corresponding to the oxygen atoms of bound nitrite at the type 2 copper site. There are also structures of NiR mutants crystallized close to active pH with more than a 20-fold excess of nitrite in which no substrate has been modeled at the type 2 copper site, possibly due to electron density peaks being assigned as water. Hence, care was taken to avoid mis-assignment of these peaks since, in principle, they could represent two solvent molecules with partial occupancy (~50% each) rather than nitrite. For example, the activity of the enzyme was assessed before crystallization setups by measuring the reoxidation of dithionite-reduced enzyme with nitrite (data not shown). As a further precaution, nitrite was added in 100-fold excess to the protein solution before mixing with precipitant solution to avoid problems with precipitants preventing nitrite binding, which has previously been reported (35). Finally, in the structure at pH 6.0, full occupancy was recovered for the oxygen atoms, and the hypothesis that they may represent two solvent molecules could, hence, be rejected because steric effects would prevent both solvent molecules to be present at the same time. When nitrite was modeled at this site the electron density became continuous, and the weaker density for the nitrogen in the $F_o - F_c$ electron density map was presumably due to the nitrogen atom being less ordered than the ligating oxygen atoms. In this context it is noted that although the position of the oxygen atoms is well conserved in all structures of NiR with bound substrate, the exact position of the nitrogen atom varies significantly (21, 36). Table 2 summarizes the processing and refinement statistics.

Downloaded from www.jbc.org at Radboud Universiteit Nijmegen, on July 12, 2012

TABLE 2
Data collection and refinement parameters
Values within parentheses show data for the last resolution shell.

	RsNiR (pH 8.4)	RsNiR + NO_2^- (pH 8.4)	RsNiR (pH 6.0)	RsNiR + NO_2^- (pH 6.0)
PDB code	1ZV2	2DWS	2DY2	2DWT
Temperature (K)	100	100	100	100
Resolution (Å)	1.74	1.85	2.26	1.90
Space group	R3	R3	R3	R3
Unit cell	$a = b = 72.4$ Å, $c = 147.5$ Å $\alpha = \beta = 90°, \gamma = 120°$	$a = b = 82.2$ Å, $c = 146.2$ Å $\alpha = \beta = 90°, \gamma = 120°$	$a = b = 75.0$ Å, $c = 153.6$ Å $\alpha = \beta = 90°, \gamma = 120°$	$a = b = 74.7$ Å, $c = 153.2$ Å $\alpha = \beta = 90°, \gamma = 120°$
Monomers/asymmetric unit	1	1	1	1
Highest resolution shell (Å)	1.74-1.81	1.85-1.92	2.26-2.38	1.90-2.00
No of observed reflections	79,426	120,914	84,764	77,758
No of unique reflections	29,034 (2,973)	30,093 (3,165)	15,031 (2,174)	25,165 (3,396)
Reflections in test set (%)	5.0	5.0	5.0	5.0
Completeness (%)	98.6 (100)	100 (100)	99.8 (100)	99.3 (100)
Redundancy	2.9 (2.7)	3.6 (3.5)	5.6 (5.6)	3.2 (3.1)
$I/\delta(I)$	9.7 (2.9)	13.3 (2.6)	7.9 (2.6)	7.2 (1.8)
*R*merge (%)	6.5 (34)	4.6 (35)	6.5 (29)	6.0 (36)
No. of solvent molecules	292	249	72	104
Mg^{2+} ions	3	0	0	0
Cu^{2+} ions	2	2	2	2
*R*work (%)	15.2	16.8	19.2	19.9
*R*free (%)	19.1	19.9	24.1	23.5
Root mean square deviation bond lengths (Å)	0.012	0.013	0.014	0.020
Root mean square deviation bond angles (°)	1.4	1.6	1.6	1.9
Average B factor	15.0	25.6	42.2	33.1
Ramachandran plot				
Residues in most favored regions (%)	90.2	89.1	86.5	88.4
Residues in additionally allowed regions (%)	9.8	10.9	13.5	11.6

Redox titration in combination with EPR spectroscopy were performed essentially as described by Olesen *et al.* (9). The concentration of type 1 copper was determined at 590 nm using an absorption coefficient of 2300 $M^{-1}cm^{-1}$ (9). Protein samples at pH 6.0 and 8.4 were prepared using 0.1 M MES and Tris, respectively. The type 1 copper concentration was estimated to be 0.3 mM at both pH 6.0 and 8.4. Ascorbic acid and potassium ferricyanide were used as reductant and oxidant, respectively, throughout the titration. *N*,*N*,*N*′,*N*′-tetramethyl-*p*-phenylenediamine and 2,6-dichlorophenol-indophenol were used as mediators at micromolar concentrations. Samples were prepared in a glove box (Belle Technology) at an oxygen level less then 5 ppm. Titrations were performed by gradually adding ascorbic acid to a larger batch of protein that had been fully oxidized with ferricyanide. The sample was allowed to equilibrate with the platinum redox electrode for more than 15 min after each addition. Small aliquots were then transferred to calibrated EPR tubes and frozen in liquid nitrogen. EPR spectra were recorded at 133 K with a Bruker Elexsys E500 spectrometer operating at 9.3 GHz. The modulation amplitude was 3.0 millitesla, and the microwave power was 21 milliwatts. The concentration of RsNiR type 2 copper was determined by integrating the first EPR hyperfine peak with the Bruker Xepr software.

FTIR spectra were obtained with a Bruker IFS-66 FTIR spectrometer (Ettlingen, Germany) equipped with a liquid nitrogen-cooled, narrow band MCT detector and interfaced to a microcomputer. Acquisition parameters were: resolution, 4 cm^{-1}; number of co-added interferograms, 1024; moving mirror velocity, 4.11 cm/s; acquisition time, 75 s. Peak to peak noise levels between 2200 and 2000 cm^{-1} were found to be less than 5×10^{-5} *A* units in all cases. Where necessary, second derivative spectra smoothed over 13 data points were calculated to resolve overlapping bands. Spectra of aqueous solution of RsNiR (2.4 mM) were obtained using a horizontal ATR (attenuated total reflectance) with a germanium internal reflection element (model A737, Bruker) and equipped with a dialysis membrane to enable changing the pH of the sample *in situ*. The pH-dependent binding of nitrite to the enzyme (2.4 mM) at 293 K was monitored in a downward and an upward pH gradient between pH 8.6 and 5.5, employing either a phosphate buffer or a HEPES (pH 8.6-7.0) plus MES buffer (pH 6.6-5.5) at a concentration of 50 mM containing 2.5 mM sodium nitrite. 50 ml of this buffer solution was superfused over the enzyme solution so as to ensure an excess substrate over enzyme. The buffer composition was chosen such that the results could be compared with the kinetic data on the overall reaction, obtained by Olesen *et al.* (9) and Zhao *et al.* (9, 23). An aqueous solution of 100 mM $NaNO_2$ shows a broad absorption around 1237 cm^{-1} (bandwidth 78 cm^{-1}) corresponding to an anti-symmetric stretching vibration within the V-shaped nitrite anion. Taking ^{15}N stable isotope-labeled nitrite, this band shows a downshift toward 1209 cm^{-1} (bandwidth 64 cm^{-1}). To diminish the effect of overlapping bands, absorbance changes induced by a downward pH gradient scan were quantified using second derivative spectra (Fig. 1*B*). Such spectra show a decreasing, negative signal at 1237 cm^{-1} flanked by two exchanging bands at 1247 and 1224 cm^{-1} (isosbestic point at 1232 cm^{-1}), resulting from the sulfonate moiety in the HEPES or MES buffer. To positively identify nitrite specific signals, the experiment was repeated using ^{15}N-labeled nitrite as a ligand. In this case, the intensity at 1237 cm^{-1} remained nearly constant, but a new signal decreasing with pH was observed at 1209 cm^{-1} (Fig. 1*D*). Upon

Downloaded from www.jbc.org at Radboud Universiteit Nijmegen, on July 12, 2012

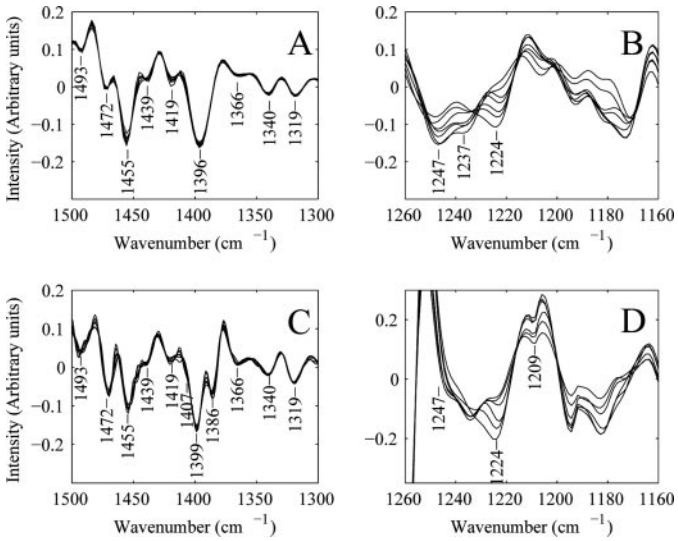

FIGURE 1. **pH dependence of substrate binding to the type 2 copper site assigned using FTIR spectroscopy.** Second derivative spectra are used for analyses to reduce spectral overlap. *A*, identification of bound, natural abundance nitrite signals was not successful. At 1366 cm^{-1} and above 1400 cm^{-1}, band intensities increase upon lowering the pH, but none of these signals can be assigned to bound nitrite. *B*, binding of natural abundance nitrite to NiR with decreasing pH results in a decreasing signal at 1237 cm^{-1}, corresponding to the free nitrite in solution. Bands at 1247 and 1224 cm^{-1} result from the sulfonate moiety in the applied buffer compounds. *C*, pH-dependent binding of ^{15}N-labeled nitrite to NiR. A new signal, increasing with decreasing pH, is observed at 1386 cm^{-1}. The shoulder at 1407 cm^{-1}, which remained unresolved in panel *a*, has disappeared. *D*, binding of ^{15}N-labeled nitrite to NiR with decreasing pH shows a decreasing signal at 1209 cm^{-1}. Bands at 1247 and 1224 cm^{-1} result from the sulfonate moiety in the applied buffer compounds.

increasing the pH in an upward gradient, release of nitrite was not observed (data not shown).

In addition, we looked for signals representing the nitrite bound to the type 2 copper site. If nitrite binds to NiR through formation of a copper-oxygen bond, the nature of the two NO bonds changed to 1, with an N═O bond characteristic and 1 with an N—O characteristic. In the infrared spectrum, these bands were expected to occur between 1500 and 1400 cm^{-1} and between 1100 and 1000 cm^{-1}, respectively. Other characteristics should be the pH dependence of the peak intensity and the shift to a lower wavenumber upon labeling the ligand with the ^{15}N stable isotope. Fig. 1, *A* and *C*, show the second derivatives of the pH-dependent infrared spectra in the range in which the N═O stretching vibrational band is expected to occur. When using natural abundance nitrite as a ligand, the bands at 1366, 1419, 1439, 1455, and 1472 cm^{-1} do show pH-dependent intensity changes (Fig. 1*A*). However, these bands cannot be assigned to an N═O vibration since the same changes were observed when using ^{15}N-labeled nitrite (Fig. 1*C*). In the latter case a new band at 1386 cm^{-1} was observed that gains intensity upon decreasing the pH. Moreover, the band originally at 1396 cm^{-1} shows a decreased bandwidth. These results can be explained by assigning the band at 1386 cm^{-1} to the N═O stretching vibration in ^{15}N-labeled nitrite, bound to the type 2 copper center. Using the harmonic oscillator approximation, the maximum frequency for the natural abundance, ^{14}N nitrite is calculated to be 1411 cm^{-1}. This value corresponds well with the unresolved shoulder at 1407 cm^{-1} found in the spectra of natural abundance nitrite bound to NiR. Further support for this assignment comes from the observation that these signals disappear upon reduction of the formed complexes by the addition of either ascorbate or sodium dithionite solutions (data not shown).

RESULTS AND DISCUSSION

Four structures of RsNiR have been solved to high resolution; at two pH values (8.4 and 6.0) and with or without nitrite. All structures crystallize in the same space group with one monomer in the asymmetric unit and were solved in a range from 1.74 to 2.26 Å resolution. When comparing all four structures, almost all significant differences are located in the immediate vicinity of the active site. These active-site structural variations observed at high resolution are detailed below and provide new insight into the pH dependence of the enzyme activity and nitrite affinity. The most noteworthy structural difference away from the active site is that, in the pH 8.4 structure without nitrite, a Mg^{2+} ion binds to residues 220 and 224 and thereby stabilizes a protruding loop (12). At pH 6.0, however, even though the $MgCl_2$ concentration is almost doubled in the crystallization conditions, no Mg^{2+} ion is visible in the structure.

Fig. 2 shows the $2F_o - F_c$ electron density map of the active site when NiR was co- crystallized with nitrite at pH 8.4 and 6.0. At pH 8.4 the substrate can only be modeled in the active site with a partial occupancy of 0.5 (Fig. 2*b*), whereas nitrite can be seen to ligate the copper ion at full occupancy at pH 6.0 (Fig. 2*a*). It should also be noted that the occupancy of nitrite may actually be lower than 0.5 in the high pH structure, since the presence of solvent ligands in the absence of nitrite may somewhat enhance the apparent occupancy of nitrite recovered through structural refinement. These observations indicate that the substrate affinity for the copper active site decreases significantly with pH, which is consistent with the results of the FTIR analyses (see below).

In either structure with (Fig. 2) or without (Fig. 3) nitrite the catalytic histidine residue, His-287, is disordered at pH 8.4 but not at pH 6.0. This disorder is most likely due to alterations in H-bonding properties because of deprotonation of the imidazole ring at high pH but possibly also due to changes in the preferred copper coordination geometry. At pH 6.0 this disordering is not seen, strengthening the hypothesis that His-287 is kept away from the copper ion by forming a H-bond to the bridging water (12) (Fig. 2*b*). From an earlier electron density map we suggested that the disorder of His-287 in RsNiR could be modeled as a dual conformation of the imidazole ring, with one conformation close to and one distant from the copper ion (12). However, the high pH structures in this paper indicate that two conformations may be a simplification of the full motion. We also previously suggested that a dual-conformational state of His-287 may prevent nitrite from binding to the active site due to a steric clash with nitrite when the imidazole ring would occupy the conformation closest to the copper ion (12). However, in our structure at pH 8.4 co-crystallized with nitrite, a nitrite molecule is modeled bound to the type 2 copper ion with an occupancy of 0.5 (Fig. 2*b*), indicating that nitrite affinity is not negligible even when His-287 is disordered.

Downloaded from www.jbc.org at Radboud Universiteit Nijmegen, on July 12, 2012

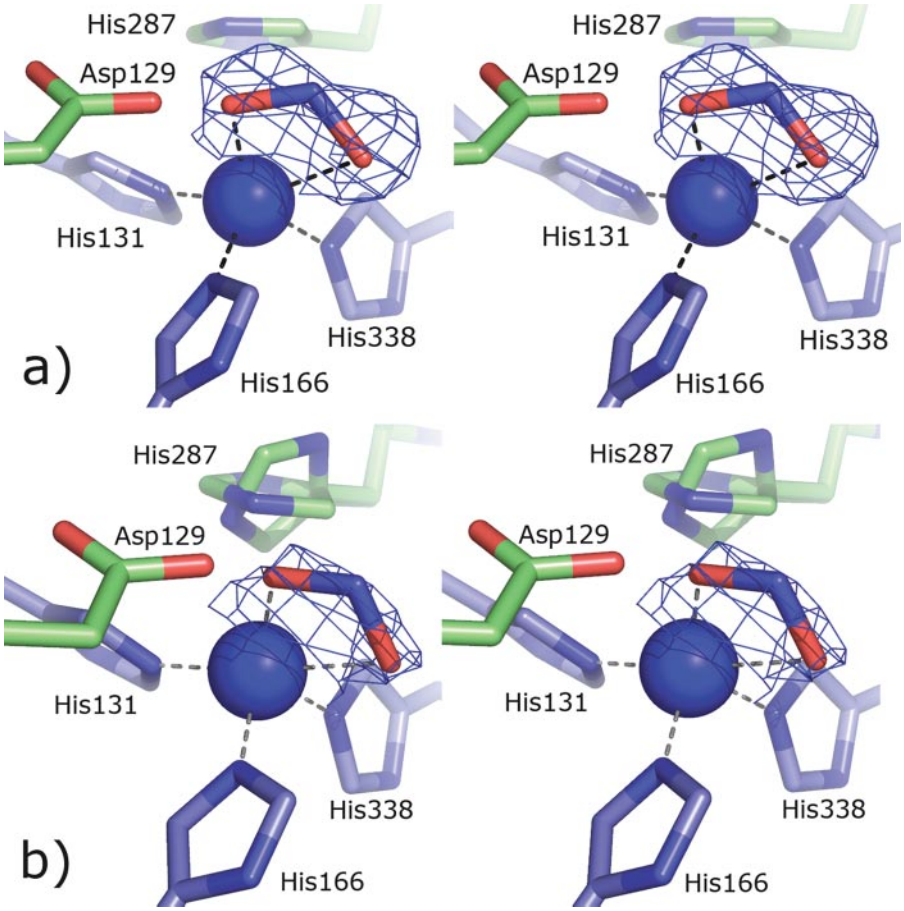

FIGURE 2. **Stereo view of nitrite bound to the type 2 copper ion in RsNiR.** *a*, at pH 6.0 showing full occupancy and with $2F_o - F_c$ electron density contoured at σ level 1.0. *b*, at pH 8.4 with half-occupancy and with $2F_o - F_c$ electron density contoured at σ level 0.9. The flexibility of His-287 at pH 8.4 can be seen as a rotation of the imidazole ring (*b*).

In the x-ray structures of RsNiR crystallized without substrate, a single water ligand was seen to be present at the active site (Fig. 3). However, this solvent molecule was located at different positions depending upon the pH, establishing that the preferred type 2 copper site geometry is pH-dependent. Similar findings have been reported for NiR from *Alcaligenes xylosoxidans*, where structures have been determined at pH 8.5 (1.9 Å of resolution; Protein Data Bank (PDB)code 1hau (37)) and pH 6.5 (1.04 Å of resolution; PDB code 1oe1 (38)). Specifically, at pH 6.5, one solvent molecule ligates the type 2 copper of *A. xylosoxidans* NiR at a position equivalent to that observed for RsNiR at pH 6.0 (Fig. 3*a*). However, at pH 8.5, two active-site water molecules are modeled with equal occupancy, one at the position found at low pH and a second at a position equivalent to that observed for RsNiR at pH 8.4 (Fig. 3*b*). Furthermore, these structural observations are consistent with a theoretical study by Källrot *et al.* (39) which shows that there are two energetically distinct preferred type 2 copper site geometries depending on the protonation state of the solvent ligand, its H-bond interactions, and the intrinsic preferences of the copper site. A change in position of the solvent ligand has been noted in an earlier mutational study where the H-bond to the catalytic aspartate was lost upon substitution to an asparagine (21). To quantify the extent to which the tetrahedral type 2 copper site geometry is distorted, the angle φ between the two planes N_{338}-Cu-O and N_{131}-Cu-N_{166} is measured (residues are numbered according to RsNiR). Källrot *et al.* (39) propose two structures for the type 2 copper site in NiRs, one that is almost perfectly tetrahedral with a φ angle close to 90° like the copper site in NiR from *Achromobacter cycloclastes* (6) and one that is more distorted and thereby less tetrahedral with a smaller φ angle, like the structure in NiR from *Alcaligenes faecalis* (40). They further suggest that these two solvent ligand positions are equally favored if the solvent ligand is a hydroxyl ion and the catalytic aspartate residue is protonated, but when the pH is such that the ligand is protonated the more tetrahedral geometry is energetically preferred. Comparing the solvent ligand positions in the RsNiR structures at pH 8.4 and 6.0 (Fig. 3), it can be seen that the solvent position at high pH adopts a less tetrahedral copper site geometry with at φ angle of 77°, whereas the solvent position at pH 6.0 promotes a more tetrahedral copper site φ angle of 87°.

Our essential finding that the preferred locations of solvent molecules ligating the type 2 copper is pH-dependent is in qualitative agreement with the theoretical studies of Källrot *et al.* (39). Quantatively, however, we observe one predominant solvent ligand position in the RsNiR structures at high pH as opposed to the two equally favored ligand positions suggested from theoretical studies. Because it seems certain that Asp-129 is deprotonated in the structure recovered at pH 8.4, we take the interpretation that the H-bond between the solvent ligand and the catalytic Asp residue is lost due to the lack of a proton in the crystal structure at high pH. This allows the solvent ligand to move slightly and thereby achieve a distorted tetrahedral type 2 copper site. This interpretation differs only minimally from the suggestion of Källrot *et al.* (39) that this H-bond should be weakened at high pH and is consistent with the x-ray structure of the type 2 copper site when the catalytic Asp was mutated to Asn (21). Furthermore, assuming that this H-bond does not exist when the solvent ligand is deprotonated allows us to reinterpret the two alternate water positions seen in the difference maps for the structure of NiR from *A. faecalis* (Protein Data Bank code 2NRD) (39) as arising from a dynamic equilibrium between the protonated and deprotonated solvent ligand species.

It is highly significant that the two distinct positions of the solvent ligands in the high and low pH structures without

Downloaded from www.jbc.org at Radboud Universiteit Nijmegen, on July 12, 2012

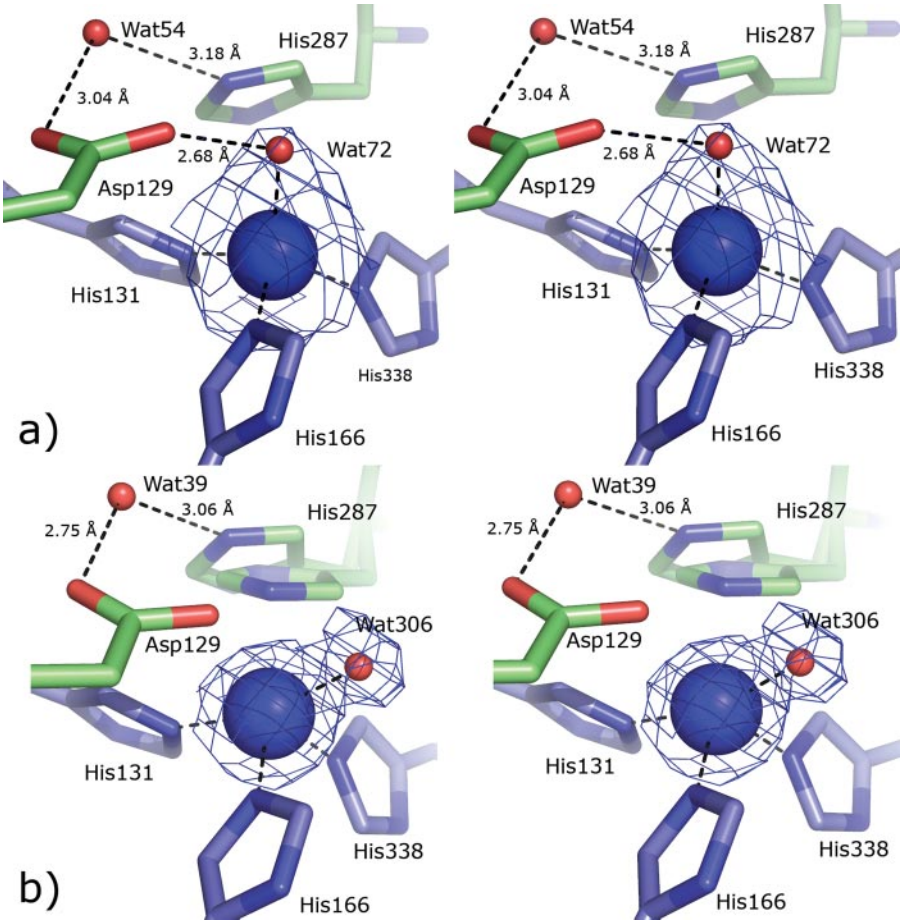

FIGURE 3. **Stereo view illustrating the ligating solvent molecule that coordinates the oxidized type 2 copper ion in Cu-NiRs.** *a* and *b*, pH 6 (*a*) and at pH 8.4 (*b*), both with $2F_o - F_c$ electron density contoured at σ level 1.0. Asp-129 forms an H-bond to the solvent ligand at pH 6.0 (*a*), but this bond is absent at pH 8.4 (*b*). The flexibility of His-287 at pH 8.4 can be seen as a movement of the imidazole ring toward the type 2 copper ion (*b*).

nitrite coincide with the positions of the oxygen atoms of bound nitrite in both RsNiR structures co-crystallized with nitrite (Fig. 4). It has previously been described that nitrite affinity is dependent upon pH such that it is maximal at approximately the pH where the enzyme activity is at its highest but decreases to negligible levels as the pH is increased (25). The fact that the two favored solvent ligand positions overlap with the oxygen positions of bound nitrite leads us to postulate that the affinity of nitrite for the type 2 copper ion is decreased if any one of these positions is energetically unfavorable. At high pH a tetrahedral solvent ligand position is disfavored according to the argument given above that no H-bond exists between the solvent ligand and Asp-129, and this would consequently lower the affinity of nitrite to the type 2 copper ion. Thus, the specific preferences of the ligand positions at the type 2 site can be coupled to nitrite affinity and its pH dependence.

To characterize the pH dependence of nitrite affinity more directly, we performed FTIR studies on RsNiR in solution. The pH dependence of nitrite binding to the type 2 copper ion was monitored during a downward pH gradient scan as a decrease in free nitrite absorbance at 1237 cm^{-1} (^{14}N) or 1209 cm^{-1} (^{15}N). The resulting sigmoid curve (Fig. 5) yields a p*K* value of 7.4 ± 0.1 that corresponds to the pH at which half-maximal binding of nitrite to NiR should occur. These results could be confirmed by monitoring the pH-dependent signal at 1386 cm^{-1}, which represents bound ^{15}N nitrite by its N═O stretching vibration. When plotting the intensity change at 1386 cm^{-1} as a function of pH, a sigmoid curve was obtained, again showing a p*K* value of 7.4 (Fig. 5). We were unable to identify in this way the N—O stretching vibration of the enzyme-bound nitrite between 1100 and 1000 cm^{-1}, since this spectral range was dominated by buffer and protein absorptions. Although previous studies have discussed the binding of nitrite inferred from a perturbation to the type 2 copper EPR signal (9, 23), the FTIR spectroscopy measurements presented here provide a more direct spectroscopic identification of nitrite binding to copper, since the signal derives from the nitrite ligand. The pH dependence of the reduction of nitrite to nitric oxide shows an optimum near pH 6 (23), and the corresponding p*K* value for the midpoint activity is ~6.8. This is somewhat lower than the p*K* for the binding of nitrite to the enzyme determined here, implying that binding of nitrite is not the rate determining step for the overall reaction.

The trend, thus, observed is qualitatively in agreement with that seen crystallographically. The modeled occupancy of 0.5 for bound nitrite in the crystal structure at pH 8.4 may seem high in light of the FTIR spectroscopic results but may be explained by the possibility of solvent molecules also partially occupying the active site. Furthermore, crystallization is a dynamic process; substrate binding may stabilize the protein somewhat, and therefore, the substrate-bound form may be favored during crystallization. Hence, substrate occupancy inferred from the crystal structure need not exactly agree with that obtained for the enzyme-substrate complex in solution.

It is well known that even small changes in copper site geometry can significantly affect the redox potential of the metal site. As described above, there are two distinct geometries of the type 2 copper site that appear to depend upon the protonation state of the solvent ligand. The reduction potential of the type 2 copper site is crucial for the activity of the protein, since a lower reduction potential of the type 2 copper site relative to that of the type 1 copper site retards electron transfer. Previous measurements have led to the conclusion that the reduction potential of the type 2 copper site in RsNiR is among the lowest observed for Cu-NiRs (1, 9) and that nitrite binding to the type 2 copper site is needed to shift the balance of the copper site

Downloaded from www.jbc.org at Radboud Universiteit Nijmegen, on July 12, 2012

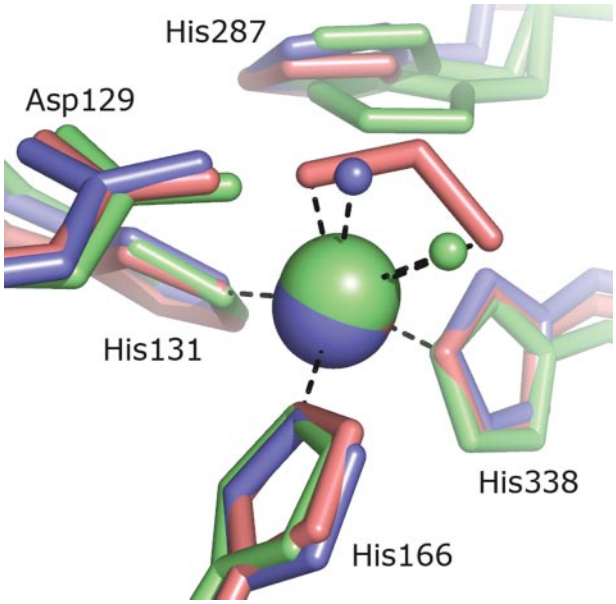

FIGURE 4. **Stereo view of RsNiR at pH 8.4 (*green*) and RsNiR at pH 6.0 (*blue*), both superimposed with the structure of RsNiR with bound nitrite at pH 6.0 (*red*).** The two solvent ligand positions (*green* and *blue*) show strong similarity to the positions occupied by the two oxygen atoms of nitrite (*red*).

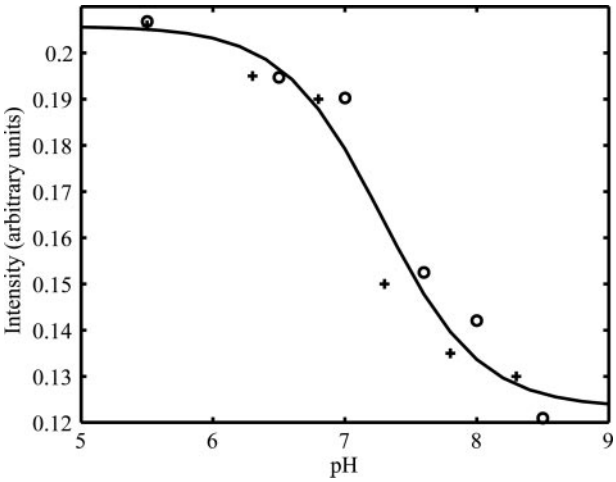

FIGURE 5. **pH-dependent binding of nitrite to the type 2 copper site in RsNiR.** The reduction of the free nitrite specific signal upon decreasing pH is monitored at 1237 cm^{-1} for natural abundance nitrite (○). The data were fitted to a four parameter sigmoidal curve using Matlab (MathWorks, Natick, MA). The fitted curve (*solid line*) shows a midpoint or pK_a at pH 7.4. Approximately the same pK_a is obtained when plotting the increase in the signal for bound ^{15}N-labeled nitrite at 1386 cm^{-1} with decreasing pH (+).

reduction potentials so as to allow electron transfer (9). Because pH-dependent changes in geometry were observed in our structures, we determined the reduction potential of the type 2 copper site using EPR at pH 6.0 and 8.4 by recording a full redox titration under anaerobic conditions.

EPR spectra of RsNiR recorded at pH 6.0 and 8.4 under different reduction potentials are shown in Fig. 6, *A* and *B*, respectively. Spectra were initially recorded from an aliquot of the fully oxidized enzyme. The sample was then stepwise reduced, the reduction potential of the solution was monitored, and aliquots were extracted, frozen, and transferred to the EPR spectrometer. A striking difference between these spectra is that a single peak at 0.265 tesla at pH 6.0 (Fig. 6*A*) is apparently split

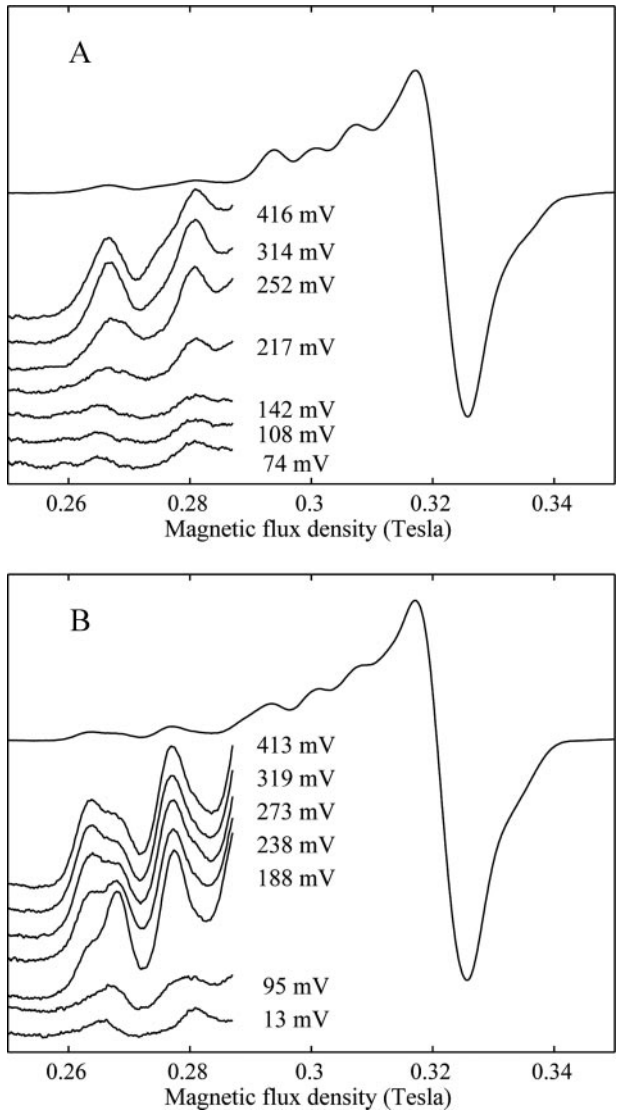

FIGURE 6. **X-band EPR spectra recorded from RsNiR at 133 K.** *A*, spectra from protein prepared at different reduction potentials at pH 6.0. *B*, spectra from protein prepared at different reduction potentials at pH 8.4. The full spectra show the completely oxidized RsNiR at 416 mV (*A*) and 413 mV (*B*). The *inset spectra* are magnified 10-fold and show the low-field region of the type 2 copper measured at the indicated reduction potentials.

into a double peak at pH 8.4 (Fig. 6*B*), indicating that two distinct copper species are present at pH 8.4. The spectral parameters of these species were as follows. At pH 6.0 the type 2 copper species has $g_\perp = 2.07$, $g_\parallel = 2.31$, and $A_\parallel = 15.0$ millitesla, and at pH 8.4 the same copper species was observed, but there was an additional type 2 copper species with $g_\perp = 2.09$, $g_\parallel = 2.35$, and $A_\parallel = 9.5$ millitesla. These observations may correlate with the observed distortion of the type 2 copper site geometry at high pH; specifically, the disordering of His-287 and the shift in solvent ligand position (Fig. 3). From the integration of the single peak at 0.265 tesla at pH 6.0 and the corresponding double peak at pH 8.4, the fraction of oxidized type 2 copper atoms was determined. These results are summarized as a redox titration curve in Fig. 7. A nonlinear fit to the Nernst equation results in midpoint potentials of 218 mV at pH 6.0 and 137 mV at pH 8.4. The fit also yielded $n = 0.5$ for both titrations (*i.e.* lower than the $n = 1$ value expected for a 1-electron transfer

Downloaded from www.jbc.org at Radboud Universiteit Nijmegen, on July 12, 2012

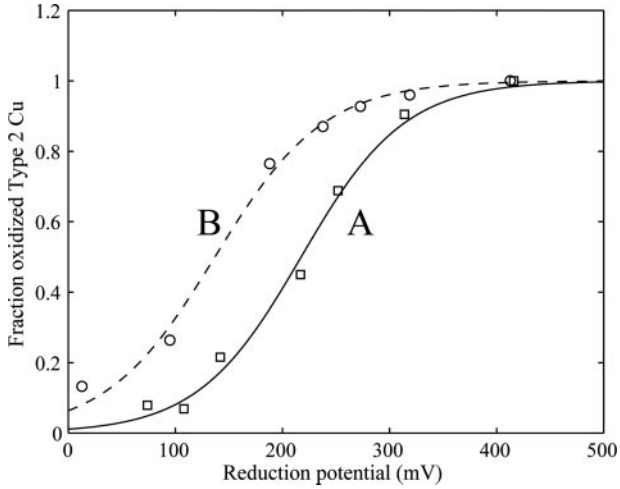

FIGURE 7. **Redox titration curves for the type 2 copper of RsNiR.** The titration curve determined from data displayed in Fig. 6*A* (pH 6.0) are shown as *squares* and that determined from data displayed in Fig. 6*B* (pH 8.4) are shown as *circles*. A best fit to the Nernst equation is also shown as a *solid line* (pH 6.0) and a *dotted line* (pH 8.4). Optimal parameters obtained from the nonlinear curve fit are $n = 0.53$ and $E_m = 218$ mV at pH 6.0 and $n = 0.51$ and $E_m = 137$ mV at pH 8.4.

reactions). This low value is most likely due to incomplete equilibration between ascorbate and RsNIR at the lower reduction potentials. Nevertheless, the pH-dependent active-site structural changes (Fig. 3) lower the midpoint potential of the type 2 copper by 81 mV. Thus, the type 2 copper is unable to accept electrons from the type 1 copper site at high pH. This may contribute to the rapid decrease in enzyme activity as the pH is increased from 6.0 to 9.0 (23, 24). Similar conclusions were drawn from studies of the change in type 2 copper site reduction potential in the Cu-NiRs from *A. xylosoxidans* and *A. cycloclastes* (1). From our structural data, an explanation for the observed decrease in redox potential of the type 2 copper site at higher pH can be hypothesized.

CONCLUSIONS

Cu-NiRs have proven to be highly pH-dependent enzymes. From a mechanistic perspective, there are several potential causes for these variations in activity with pH such as changes in the protonation state of active-site residues and solvent molecules, changes in the binding affinity of nitrite to the active-site copper, pH-dependent changes in the geometry of the type 2 copper site, and pH-dependent changes in the redox potentials affecting intramolecular electron transfer. From a physiological perspective this functional pH dependence correlates well with the observation that at high pH the expression levels of NiR within the cell are down-regulated (26). This pH-dependent NiR regulation in turn creates a feedback mechanism whereby high concentrations of nitrite cause the pH to drop, inducing the expression of NiR so as to metabolize overabundant nitrite and, thus, help raise the pH. Conversely, lowering the activity of those NiR molecules already present as the pH increases prevents them from reducing additional nitrite under these conditions and thereby achieves a more immediate response to changes in the pH than can be achieved at the transcriptional level.

Our structural findings show how the active-site geometry of nitrite-free RsNiR changes as the pH is raised or lowered and suggest that the exact position of one solvent molecule copper ligand provides a structural fingerprint enabling it to be recognized either as a water molecule or as a hydroxide ion. This finding is in accordance with theoretical studies on the pH dependence of Cu-NiRs (39). An explicit coupling between structure and activity is emphasized through additional studies showing the reduced nitrite affinity at high pH, by changes in the reduction potential of the type 2 copper ion with pH, and by the presence or absence of protons on the solvent ligands and neighboring residues of the type 2 copper ion. These findings appear to be of a rather generic nature and may, therefore, aid the understanding of the pH dependence of a broad family of other copper-dependent enzymes.

REFERENCES

1. Suzuki, S., Kataoka, K., Yamaguchi, K., Inoue, T., and Kai, Y. (1999) *Coordination Chemistry Reviews* **192,** 245–265
2. Zumft, W. G. (1997) *Microbiol. Mol. Biol. Rev.* **61,** 533–616
3. Fulop, V., Moir, J. W. B., Ferguson, S. J., and Hajdu, J. (1995) *Cell* **81,** 369–377
4. Nurizzo, D., Silvestrini, M. C., Mathieu, M., Cutruzzola, F., Bourgeois, D., Fulop, V., Hajdu, J., Brunori, M., Tegoni, M., and Cambillau, C. (1997) *Structure* **5,** 1157–1171
5. Inoue, T., Gotowda, M., Deligeer, Kataoka, K., Yamaguchi, K., Suzuki, S., Watanabe, H., Gohow, M., and Kai, Y. (1998) *J. Biochem.* **124,** 876–879
6. Adman, E. T., Godden, J. W., and Turley, S. (1995) *J. Biol. Chem.* **270,** 27458–27474
7. Dodd, F. E., Hasnain, S. S., Abraham, Z. H. L., Eady, R. R., and Smith, B. E. (1997) *Acta Crystallogr. D Biol. Crystallogr.* **53,** 406–418
8. Kukimoto, M., Nishiyama, M., Murphy, M. E. P., Turley, S., Adman, E. T., Horinouchi, S., and Beppu, T. (1994) *Biochemistry* **33,** 5246–5252
9. Olesen, K., Veselov, A., Zhao, Y. W., Wang, Y. S., Danner, B., Scholes, C. P., and Shapleigh, J. P. (1998) *Biochemistry* **37,** 6086–6094
10. Kukimoto, M., Nishiyama, M., Tanokura, M., Adman, E. T., and Horinouchi, S. (1996) *J. Biol. Chem.* **271,** 13680–13683
11. Impagliazzo, A., Krippahl, L., and Ubbink, M. (2005) *Chembiochem* **6,** 1648–1653
12. Jacobson, F., Guo, H. W., Olesen, K., Okvist, M., Neutze, R., and Sjolin, L. (2005) *Acta Crystallogr. D Biol. Crystallogr.* **61,** 1190–1198
13. Murphy, M. E. P., Turley, S., and Adman, E. T. (1997) *J. Biol. Chem.* **272,** 28455–28460
14. Godden, J. W., Turley, S., Teller, D. C., Adman, E. T., Liu, M. Y., Payne, W. J., and Legall, J. (1991) *Science* **253,** 438–442
15. Suzuki, S., Kohzuma, T., Deligeer, Yamaguchi, K., Nakamura, N., Shidara, S., Kobayashi, K., and Tagawa, S. (1994) *J. Am. Chem. Soc.* **116,** 11145–11146
16. Boulanger, M. J., Kukimoto, M., Nishiyama, M., Horinouchi, S., and Murphy, M. E. P. (2000) *J. Biol. Chem.* **275,** 23957–23964
17. Antonyuk, S. V., Strange, R. W., Sawers, G., Eady, R. R., and Hasnain, S. S. (2005) *Proc. Natl. Acad. Sci. U. S. A.* **102,** 12041–12046
18. Tocheva, E. I., Rosell, F. I., Mauk, A. G., and Murphy, M. E. P. (2004) *Science* **304,** 867–870
19. Wijma, H. J., Boulanger, M. J., Molon, A., Fittipaldi, M., Huber, M., Murphy, M. E. P., Verbeet, M. P., and Canters, G. W. (2003) *Biochemistry* **42,** 4075–4083
20. Boulanger, M. J., and Murphy, M. E. P. (2001) *Biochemistry* **40,** 9132–9141
21. Ellis, M. J., Prudencio, M., Dodd, F. E., Strange, R. W., Sawers, G., Eady, R. R., and Hasnain, S. S. (2002) *J. Mol. Biol.* **316,** 51–64
22. Veselov, A., Olesen, K., Sienkiewicz, A., Shapleigh, J. P., and Scholes, C. P. (1998) *Biochemistry* **37,** 6095–6105
23. Zhao, Y. W., Lukoyanov, D. A., Toropov, Y. V., Wu, K., Shapleigh, J. P., and Scholes, C. P. (2002) *Biochemistry* **41,** 7464–7474

Downloaded from www.jbc.org at Radboud Universiteit Nijmegen, on July 12, 2012

24. Kobayashi, K., Tagawa, S., Deligeer, and Suzuki, S. (1999) *J. Biochem.* **126,** 408–412
25. Abraham, Z. H. L., Smith, B. E., Howes, B. D., Lowe, D. J., and Eady, R. R. (1997) *Biochem. J.* **324,** 511–516
26. Beaumont, H. J. E., Lens, S. I., Reijnders, W. N. M., Westerhoff, H. V., and van Spanning, R. J. M. (2004) *Mol. Microbiol.* **54,** 148–158
27. Leslie, A. G. W. (1992) *Joint CCP4 + ESF-EAMCB Newsletter on Protein Crystallography 26*, pp. 27–33, *European Synchrotron Radiation Facility*, Grenoble, France
28. Evans, P. R. (1997) *Joint CCP4 + ESF-EAMCB Newsletter on Protein Crystallography* 33, pp. 22–24, *European Synchrotron Radiation Facility*, Grenoble, France
29. Bailey, S. (1994) *Acta Crystallogr. D Biol. Crystallogr.* **50,** 760–763
30. Navaza, J. (1994) *Acta Crystallogr. Sect. A* **50,** 157–163
31. Vagin, A., and Teplyakov, A. (1997) *J. Appl. Crystallogr.* **30,** 1022–1025
32. Murshudov, G. N., Vagin, A. A., Lebedev, A., Wilson, K. S., and Dodson, E. J. (1999) *Acta Crystallogr. D Biol. Crystallogr.* **55,** 247–255
33. Jones, T. A., Zou, J. Y., Cowan, S. W., and Kjeldgaard, M. (1991) *Acta Crystallogr. A* **47,** 110–119
34. Lamzin, V. S., and Wilson, K. S. (1993) *Acta Crystallogr. Sect. D* **49,** 129–147
35. Barrett, M. L., Harris, R. L., Antonyuk, S., Hough, M. A., Ellis, M. J., Sawers, G., Eady, R. R., and Hasnain, S. S. (2004) *Biochemistry* **43,** 16311–16319
36. Boulanger, M. J., and Murphy, M. E. P. (2002) *J. Mol. Biol.* **315,** 1111–1127
37. Ellis, M. J., Dodd, F. E., Strange, R. W., Prudencio, M., Sawers, G., Eady, R. R., and Hasnain, S. S. (2001) *Acta Crystallogr. D Biol. Crystallogr.* **57,** 1110–1118
38. Ellis, M. J., Dodd, F. E., Sawers, G., Eady, R. R., and Hasnain, S. S. (2003) *J. Mol. Biol.* **328,** 429–438
39. Källrot, N., Nilsson, K., Rasmussen, T., and Ryde, U. (2005) *Int. J. Quantum Chem.* **102,** 520–541
40. Murphy, M. E. P., Turley, S., Kukimoto, M., Nishiyama, M., Horinouchi, S., Sasaki, H., Tanokura, M., and Adman, E. T. (1995) *Biochemistry* **34,** 12107–12117

Downloaded from www.jbc.org at Radboud Universiteit Nijmegen, on July 12, 2012